Patzer, C., Tietze, K., Ritter, O. (2017): Steel-cased wells in 3-D controlled source EM modelling. - *Geophysical Journal International*, *209*, 2, pp. 813—826.

DOI: http://doi.org/10.1093/gji/ggx049

Geophysical Journal International

Geophys. J. Int. (2017) **209,** 813–826
Advance Access publication 2017 February 7
GJI Marine geosciences and applied geophysics

doi: 10.1093/gji/ggx049

Steel-cased wells in 3-D controlled source EM modelling

Cedric Patzer,[1,2] Kristina Tietze[1] and Oliver Ritter[1,2]

[1] *German Research Centre for Geosciences GFZ, Telegrafenberg, D-14479 Potsdam, Germany. E-mail: cpatzer@gfz-potsdam.de*
[2] *Department of Earth Sciences, Freie Universität, Malteserstr. 74-100, D-12249 Berlin, Germany*

Accepted 2017 February 6. Received 2017 February 1; in original form 2016 October 20

SUMMARY

Over the last decades, electromagnetic methods have become an accepted tool for a wide range of geophysical exploration purposes and nowadays even for monitoring. Application to hydrocarbon monitoring, for example for enhanced oil recovery, is hampered by steel-cased wells, which typically exist in large numbers in producing oil fields and which distort electromagnetic fields in the subsurface. Steel casings have complex geometries as they are very thin but vertically extended; moreover, the conductivity contrast of steel to natural materials is in the range of six orders of magnitude. It is therefore computationally prohibitively costly to include such structures directly into the modelling grid, even for finite element methods. To tackle the problem we developed a method to describe steel-cased wells as series of substitute dipole sources, which effectively interact with the primary field. The new approach cannot only handle a single steel-cased well, but also an arbitrary number, and their interaction with each other. We illustrate the metal casing effect with synthetic 3-D modelling of land-based controlled source electromagnetic data. Steel casings distort electromagnetic fields even for large borehole-transmitter distances above 2 km. The effect depends not only on the distance between casing and transmitter, but also on the orientation of the transmitter to the borehole. Finally, we demonstrate how the presence of steel-cased wells can be exploited to increase the sensitivity and enhance resolution in the target region. Our results show that it is at least advisable to consider the distribution of steel-cased wells already at the planning phase of a controlled source electromagnetic field campaign.

Key words: Numerical solutions; Numerical approximations and analysis; Electromagnetic theory; Non-linear electromagnetics.

1 INTRODUCTION

Controlled Source electromagnetic (CSEM) prospecting has become an established tool for a wide range of exploration targets, including marine (Constable 2010), airborne (Siemon *et al.* 2009) and cross well applications (Newman & Alumbaugh 1997). Despite all improvements during the last decade, the presence of steel-cased wells in the study area remains a challenging task for EM modelling methodologies. One reason is the huge conductivity contrast of steel (in the order of 5×10^6 S m^{-1}) to the surrounding rock formations (typically 0.01–1 S m^{-1}) (Frischknecht 1988), which can cause accuracy problems for conventional finite differences and finite element simulation techniques. The second issue is related to the unfavourable spatial dimensions of steel casings. In the horizontal direction boreholes are only a few centimetres to decimetres wide but they can extend for several kilometres vertically. Direct integration of such structures into the modelling grid results in huge meshes and is computationally extremely costly, not only for finite difference simulation but also for finite element modelling. Most previous work dealing with the influence of steel casings was therefore based on integral equation approaches. Wait & Hill (1973) considered a long vertical extended cylinder in a homogeneous half-space. Augustin *et al.* (1989) investigated how EM measurements could be carried out behind a metal casing.

More recent work by Commer *et al.* (2015) investigated the effect of a single steel-cased well on time domain electromagnetic methods by approximating the real borehole dimensions and conductivity of steel into the modelling grid. The study showed that, a steel-cased well in the vicinity of an EM source causes changes in amplitudes of the electric fields as well as reversing directions of the related electric currents in the subsurface. Commer *et al.* (2015) could also demonstrate, however, that the distortion of the EM fields by the steel casing leads to a significantly higher current concentration and thus higher resolution at reservoir level when compared to the case with absent casing. This general idea of making use of existing steel casings in exploration and monitoring goes back to the 1980s. Rocroi & Koulikov (1985) investigated if steel casings could be energized and used as vertical line sources to overcome a shielding effect of a resistive overburden for direct current measurements. Integration of such sources into modern 3-D frequency domain modelling and inversion schemes requires an accurate description of their physical behaviour. Yang *et al.* (2009) developed a method to calculate the distribution of source currents along an energized steel casing with depth for a 1-D half-space and

Pardo *et al.* (2008) investigated the sensitivity of energized steel casings to water displacement in oil bearing formations.

Feasibility studies on applicability of EM methods for hydrocarbon monitoring, that is, to image contrasts between formation water and oil over time (e.g. Orange *et al.* 2009; Wirianto *et al.* 2010), have indicated, that changes at reservoir level create rather small time-lapse signals which are challenging to resolve when using only surface transmitter and receivers. In oil fields, the reservoir is typically penetrated by many boreholes, energized steel casings can be seen as a simple and cheap way to move the EM source closer to the reservoir (e.g. Tietze *et al.* 2015) thereby enhancing sensitivity with depth.

There are two principle ways to energize steel casings: actively, by galvanic connection, or passively, coupled by electromagnetic induction. Based on an idea presented by Swidinsky *et al.* (2013), Tang *et al.* (2015) developed a method to describe a single steel-cased well as a series of substitute dipole sources. The current strength of these dipoles (source segments) is calculated assuming a homogeneous background conductivity. Most importantly, these substitute dipole sources create additional secondary electromagnetic fields which can be regarded as an update of the primary field, which is obviously very useful when working with a secondary field formulation to solve Maxwell's equations. Since the response of the steel casing becomes part of the primary field calculation there is no need for an approximation and complicated discretization of the borehole casing in FD or FE meshes. As the approach of Tang *et al.* (2015) does not make any assumptions on the actual type and location of the transmitter, it can be used for galvanically connected as well as inductively coupled wells. Oil fields typically consist of dozens or hundreds of steel-cased wells, drilled within distances of a few hundred metres. It is therefore necessary to consider mutual induction between wells.

For this paper, we expanded the algorithm of Tang *et al.* (2015) to take interaction between multiple wells into account. We implemented the new algorithm into our 3-D CSEM forward modelling (based on Streich 2009) and inversion (Grayver *et al.* 2013) algorithm and show how steel casings influence the distribution of electric fields in a synthetic 3-D modelling scenario. Furthermore we show how the sensitivity of the inversion is influenced if steel-cased wells are present.

2 METHODOLOGY

The methodology to include the effect of steel-cased wells into our 3-D finite difference controlled source electromagnetic modelling and inversion algorithm is based on an approach described by Tang *et al.* (2015). In this approach steel-cased wells are described as and substituted by a series of vertical electric dipole (VED) sources. The source current of these dipole sources is calculated from the z-component of the primary electric field at the position of the well segment produced by an arbitrary transmitter. In a second step, the additional electromagnetic field generated by these substitute dipoles is superimposed on the primary field of the transmitter. The updated primary field including the substitute dipoles can then be used for any secondary field approach in 3-D modelling or inversion.

2.1 A single steel-cased well

First, we summarize the main ideas of the method presented by Tang *et al.* (2015) which is valid for a single and perfectly vertical steel-cased well. The borehole is subdivided into N segments and it is assumed that the vertical current density $J_{z,j}$ on each segment j is constant. A sketch of one steel casing segment is shown in Fig. 1. The outer radius of the segment is given by r_a, the inner radius by r_i. Each segment has a length of dz and its centre point is located at depth z_c.

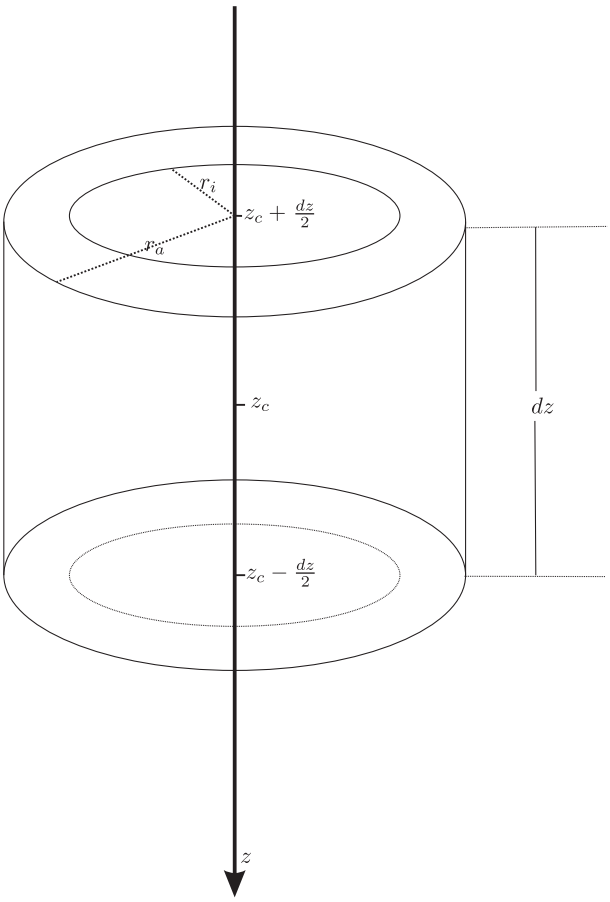

Figure 1. Sketch of one borehole segment with length dz and outer and inner radii of r_a and r_i. The centre point of the casing is located at depth z_c.

The vertical electric field at the centre point z_c of each segment j is given by the superposition of the field generated by the transmitter and the field generated by each segment of the casing:

$$E_{z,j}(z_{c,j}) = E^{\text{prime}}_{z,j}(z_{c,j}) + \sum_{k=1}^{N} E^{\text{Wells}}_{z,k}(z_{c,j}), \tag{1}$$

with $E^{\text{prime}}_{z,j}$ being the z-component of the primary electric field generated by the transmitter. Eq. (1) can be rewritten as

$$\frac{J_{z,j}}{\sigma_c} = E^{\text{prime}}_{z,j} + \sum_{k=1}^{N} J_{z,k} \iiint_{\Delta V_k} G_{zz}(x, y, z|x', y', z')\mathrm{d}V', \tag{2}$$

where $J_{z,j}$ is the vertical current density on the casing segment j, σ_c the conductivity of the casing (usually the conductivity of steel) and $G_{zz}(x, y, z, |x', y', z')$ the Green's tensor element describing the vertical electric field generated at position (x, y, z) by a VED source located at (x', y', z'). For a homogeneous half-space an analytic formulation of G_{zz} was given by Raiche & Coggon (1975):

$$G_{zz}(x, y, z|x', y', z') = \frac{1}{4\pi\sigma_b} \int_0^\infty \frac{k^3}{s} J_0(kr)(e^{-s|z-z'|} - e^{-s|z+z'|})\mathrm{d}k \tag{3}$$

with s being

$$s = \sqrt{k^2 - i\omega\mu\sigma_b}. \tag{4}$$

σ_b is the conductivity of the half-space, μ the magnetic permeability which is assumed to be the permeability of vacuum, ω the angular frequency and i the imaginary unit. J_0 refers to the Bessel function of the first kind and order zero and r is the horizontal distance between source and receiver

$$r = \sqrt{(x - x')^2 + (y - y')^2}. \tag{5}$$

A time dependency of $e^{-i\omega t}$ is assumed implicitly. After some rearrangements, eq. (2) can be expressed as system of linear equations of the form:

$$\mathbf{A}\mathbf{J_z} = \mathbf{E_z^{prime}}. \tag{6}$$

The diagonal elements of $\mathbf{A}$ are given by

$$\begin{aligned} A_{ii} = {} & \frac{1}{\sigma_c} - \frac{r_a}{2\sigma_b}\int_0^\infty \frac{k^2}{s^2}\left(2e^{-s\frac{dz}{2}} - 2 - e^{-s(2z_c+\frac{dz}{2})}\right) J_1(kr_a)\mathrm{d}k \\ & + \frac{r_i}{2\sigma_b}\int_0^\infty \frac{k^2}{s^2}\left(2e^{-s\frac{dz}{2}} - 2 - e^{-s(2z_c+\frac{dz}{2})}\right) J_1(kr_i)\mathrm{d}k, \end{aligned} \tag{7}$$

and the non-diagonal elements result in

$$\begin{aligned} A_{ij} = {} & -\frac{r_a}{2\sigma_b}\int_0^\infty \frac{k^2}{s^2}\left(e^{-s(|z_i-z_j|+\frac{dz}{2})} - e^{-s(|z_i-z_j|-\frac{dz}{2})}\right. \\ & \left. - e^{-s(z_i+z_j+\frac{dz}{2})} + e^{-s(z_i+z_j-\frac{dz}{2})}\right) J_1(kr_a)\mathrm{d}k \\ & + \frac{r_i}{2\sigma_b}\int_0^\infty \frac{k^2}{s^2}\left(e^{-s(|z_i-z_j|+\frac{dz}{2})} - e^{-s(|z_i-z_j|-\frac{dz}{2})}\right. \\ & \left. - e^{-s(z_i+z_j+\frac{dz}{2})} + e^{-s(z_i+z_j-\frac{dz}{2})}\right) J_1(kr_i)\mathrm{d}k. \end{aligned} \tag{8}$$

Solving the system of equations given in eq. (6), we obtain the current density J_z for each well segment. The source current strength of each substitute dipole can be derived using

$$I_z = \pi\left(r_a^2 - r_i^2\right) J_z. \tag{9}$$

Finally, the additional dipole sources are used to calculate an update of the primary field prior to the 3-D secondary field forward simulation.

2.2 Multiple coupled wells

In presence of more than one well, the effect of the steel casings is interrelated and the current distribution on each well depends not only on the transmitter and the conductivity but also on the geometries of the other wells. In active oil fields the number can easily exceed 100 in an area of only a few square kilometres. Hence, we extended the approach described above to consider the interaction of multiple wells. The response of multiple wells and their interaction with each other can be incorporated if matrix $\mathbf{A}$ is expanded to $M \times M$ blocks, where M stands for the number of wells:

$$\mathbf{A} = \begin{pmatrix} \mathbf{A}_{11} & \mathbf{A}_{21} & \dots & \mathbf{A}_{M1} \\ \mathbf{A}_{12} & \mathbf{A}_{22} & \dots & \mathbf{A}_{M2} \\ \vdots & \vdots & \ddots & \vdots \\ \mathbf{A}_{1M} & \mathbf{A}_{2M} & \dots & \mathbf{A}_{MM} \end{pmatrix}. \tag{10}$$

The diagonal blocks $\mathbf{A}_{ii}$ describe the interaction of all segments within the same borehole i with each other, that is, the effect of a single well as described in Section 2.1. All other blocks $\mathbf{A}_{ij}$ where $i \neq j$ describe the interaction between any two wells i and j. For the calculation of the entries in the off-diagonal blocks we follow the general idea of eq. (2). Since the horizontal distances between two well segments is much larger than the horizontal dimensions of the well itself, integration over the Green's tensor in horizontal dimensions can be neglected. Hence, electrical currents can be assumed to resemble a vertical line source located at the centre of the segment:

$$A_{ij} = \pi\left(r_a^2 - r_i^2\right)\int_{z_i-\frac{dz}{2}}^{z_i+\frac{dz}{2}} G_{zz}(x_j, y_j, z_j|x_i, y_i, z')\mathrm{d}z', \tag{11}$$

which leads to

$$\begin{aligned} A_{ij} = {} & \frac{r_a^2 - r_i^2}{4\sigma_b}\int_0^\infty \frac{k^3}{s^2}\left(2 + e^{-s(z_j+z_i+\frac{dz}{2})} - e^{-s(z_j+z_i-\frac{dz}{2})}\right. \\ & \left. - e^{-s(z_j-z_i+\frac{dz}{2})} - e^{-s(-z_j+z_i+\frac{dz}{2})}\right) J_0(kd)\mathrm{d}k, \end{aligned} \tag{12}$$

if $z_i - \frac{dz}{2} < z_j < z_i + \frac{dz}{2}$ and otherwise

$$\begin{aligned} A_{ij} = {} & \frac{r_a^2 - r_i^2}{4\sigma_b}\int_0^\infty \frac{k^3}{s^2}\left(e^{-s(|z_i-z_j|+\frac{dz}{2})} - e^{-s(|z_i-z_j|-\frac{dz}{2})}\right. \\ & \left. - e^{-s(z_i+z_j+\frac{dz}{2})} + e^{-s(z_i+z_j-\frac{dz}{2})}\right) J_0(kd)\mathrm{d}k \end{aligned} \tag{13}$$

for all segments i and j that do not belong to the same well. Here d denotes the horizontal distance between the two boreholes.

2.3 Implementation

Matrix $\mathbf{A}$ describing the interaction between the boreholes is independent of the actual transmitter and can be therefore used for any type of EM transmitter, including electric or magnetic sources of any location and orientation. Hence, for a given set of boreholes matrix $\mathbf{A}$ has to be calculated only once for each frequency. Then, the system of equations in eq. (6) has to be solved for many right hand side vectors (one for each transmitter) using an LU decomposition. Note, $\mathbf{A}$ is complex, full and in general not symmetric.

Let us assume M boreholes which are subdivided into N segments each. In order to calculate matrix $\mathbf{A}$, $N^2(M^2 + M)$ Hankel integrals have to be computed for each frequency used in the simulation, which can be numerically challenging and time consuming. The number of Hankel transformations can be reduced significantly, however, by making use of symmetries within $\mathbf{A}$. All possible symmetries that can occur are summarized in Fig. 2.

Let us consider four borehole segments i, j, k and l, where i and j belong to the one well and k and l to a second steel casing. If the pair of segments i and k of different boreholes are positioned at the same depth (z_c), have the same radii (r_a) and (r_i) as well as length (dz) and the same is valid for segments j and l, then several entries in the coupling matrix $\mathbf{A}$ only need to be calculated once. In this particular case the number of independent entries is reduced from 16 to 8 (*cf.* Fig. 2). In the most extreme scenario where all wells are identical, except for the horizontal position, the only coupling terms in $\mathbf{A}$ that have to be calculated are the upper off-diagonal blocks in eq. (10) plus one block on the main diagonal which results in a symmetric matrix $\mathbf{A}$.

3 SIMULATION EXAMPLES

The current strength along the boreholes depends on the distribution of the electric field in the z-direction produced by the EM source (transmitter). Fig. 3 illustrates the qualitative distribution of the electric field for an extended horizontal electric dipole at

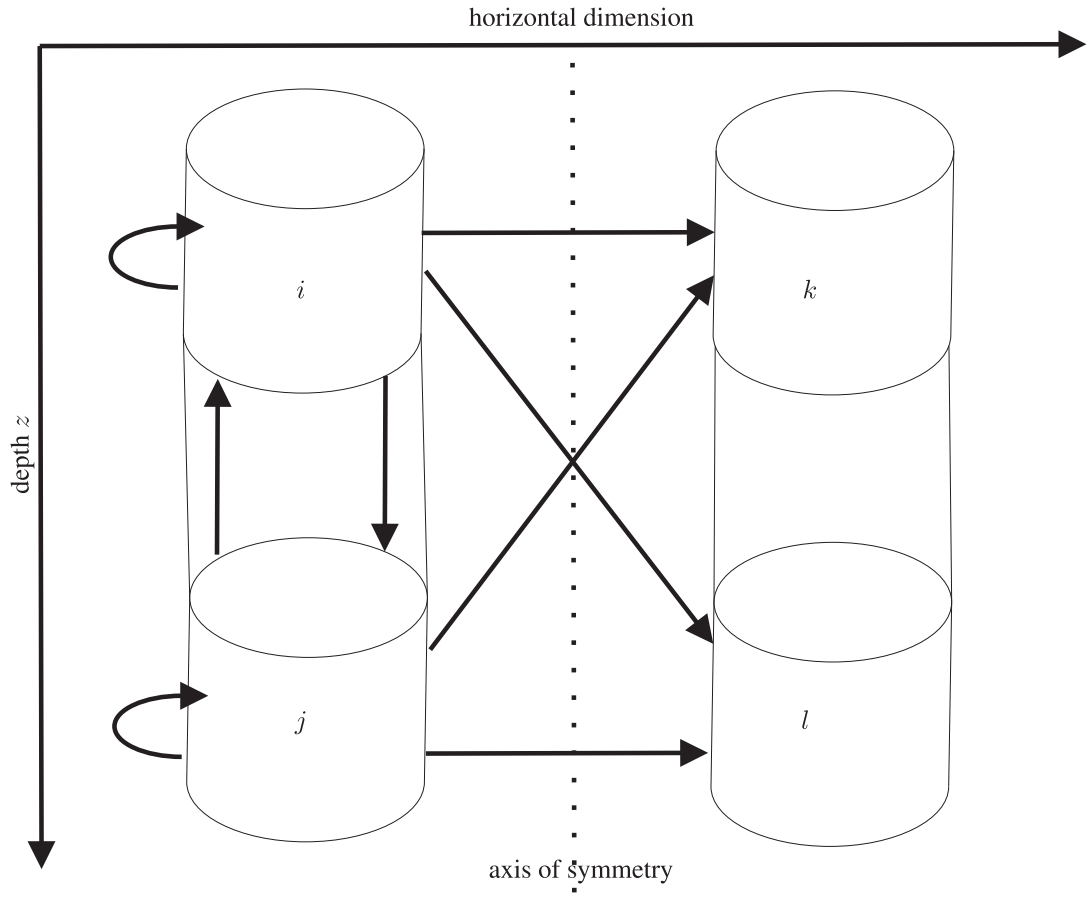

Figure 2. Sketch indicating symmetries between coupling coefficients in matrix **A** for four borehole segments belonging to two different boreholes. Segment *i* is positioned in the same depth as segment *k* and the same is true for segments *j* and *l*. Each arrow indicates one independent coefficient of **A**. The eight missing arrows are redundant due to rotational symmetry along the axis of symmetry indicated by the dotted line.

surface. All three field components are strongest at the transmitter position, which is indicated by highly saturated (red and blue) colours. Field amplitudes decrease rapidly with increasing distance to the transmitter, indicated by fading colours. Some distributions of the field components become zero at axes and planes of symmetry. Most prominent symmetry is the plane normal to the transmitter axis, marked by a green dashed line in Figs 3(b)–(d). Along this plane, both the *y*- and the *z*-component become zero, while the *x*-component (Fig. 3a) has its maximum. This plane of symmetry also marks polarity reversals of the associated fields, indicated by transition from red to blue colours. For E_z polarity is not only changing with respect to the orientation of the transmitter, but also with depth (Fig. 3d). The resulting image reveals cells of positive and negative polarity alternating with depth and gradually decreasing amplitudes; the higher the conductivity of the subsurface and the higher the frequency, the smaller their amplitudes become.

3.1 Verification against finite element modelling

We cross-checked our analytical solution with finite element (FE) modelling. At first, we tested the solution for a single steel-cased well. Due to computational limitations we could not discretise a borehole with realistic dimensions (e.g. diameter of 20 cm and wall thickness of 2 cm). Instead, we approximated the well as a highly conductive full cylinder embedded in a homogeneous half-space. The cylinder has a radius of 1 m and a length of 1300 m. Since the cross-sectional area of the cylinder is much larger than that of a true steel casing, we decreased the conductivity from that of steel (5×10^6 S m^{-1}) to 17 500 S m^{-1}; the half-space conductivity was set to 0.33333 S m^{-1}. A 1 km long grounded electric dipole was placed at surface, 500 m away from the borehole centre. The FE simulations were calculated using the Comsol Multiphysics Software package. The final mesh consisted of 1 010 096 tetrahedrons. The elements describing the cylinder have volumes in the order 0.0630 m^3.

Fig. 4 compares the FE results for the current along the casing with our new approach. Note, if the inner radius is set to zero, the integrand in eqs (7) and (8) becomes singular although the integral itself is well behaved, therefore we set the inner radius of the casing to $r_i = 10^{-8}$ m. The FE mesh had to be made very fine inside the cylinder to address the strong gradient of the electric field at the well-rock boundary as well as inside the casing. This contrast in element volume results in poor mesh quality factors which prohibits the use of the default iterative solvers. Therefore we used the MUMPS direct solver for the solution of the linear system of equations. The solution obtained by FE modelling contains significant amounts of numerical noise, but overall results are in good agreement with the new semi-analytic approach. The finite element simulation took approximately 8 hr of computing time for a single steel-cased well and required approximately 90 GB of RAM. Our new approach took less than a minute on a standard PC.

We also tested our new method for multiple wells. For the finite element simulation, two conductive cylinders of 1 m radius each were placed inside a 3 Ωm half-space. Both cylinders were aligned

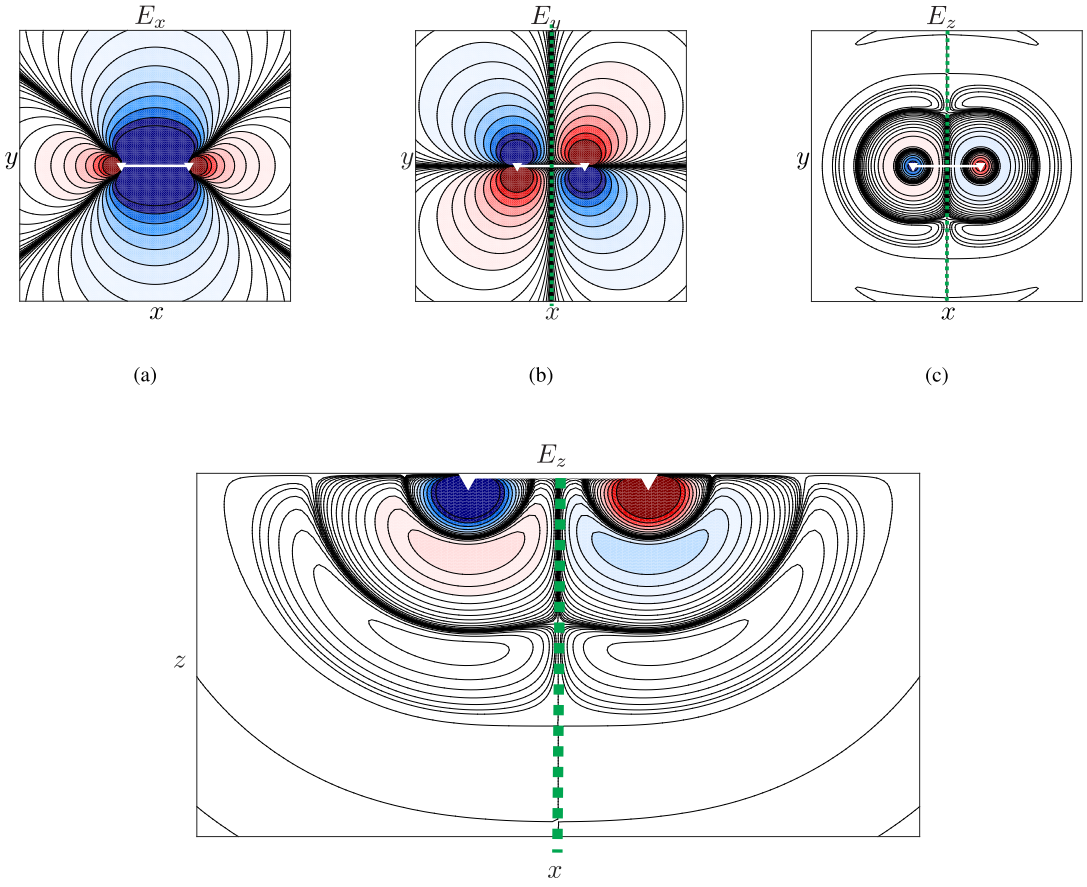

Figure 3. Qualitative distribution of the electric field (E_x, E_y, and E_z components) for an extended horizontal electric dipole source at surface of a homogeneous half-space. The dipole position is shown in white colour and its axis is aligned with the x-direction. Colours represent the polarity of the field (red positive, blue negative) and the colour saturation indicates the amplitude of the field. (a) Map view of the real part of the electric field in the x-direction. (b) Map view of the real part of the electric field in the y-direction. (c) Map view at some depth of the real part of the electric field in the z-direction. (d) Distribution of the real part of the electric field in the z-direction along the xz-plane beneath the transmitter.

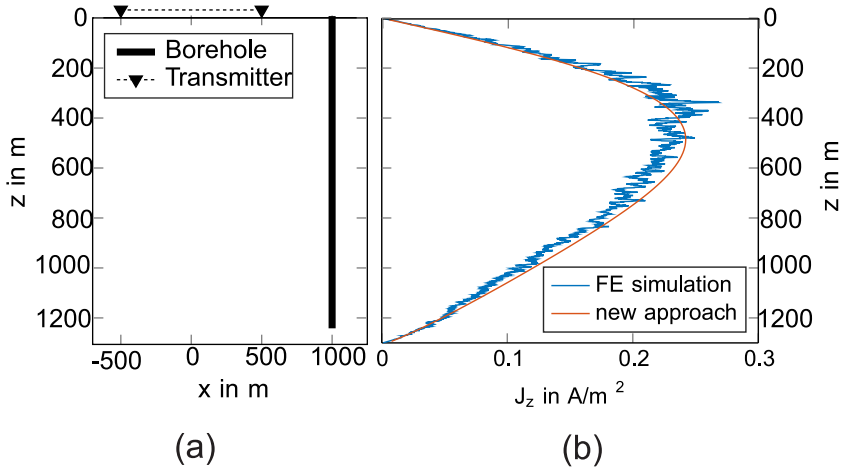

Figure 4. Comparison of our new approach to FE modelling. (a) The casing is approximated as a full cylinder of 1 m radius with a conductivity of 17 500 S m^{-1}. The cylinder reaches to a depth of 1300 m and is placed at 500 m distance to the transmitter. The source is a grounded horizontal electric dipole of 1000 m length at surface and current on the transmitter is 40 A. The background resistivity was set to 3 Ωm. (b) Current density along the conductive cylinder for a transmitter frequency of 1 Hz. Shown in blue colours are results obtained from FE simulations, red colours indicate the outcome using our new algorithm.

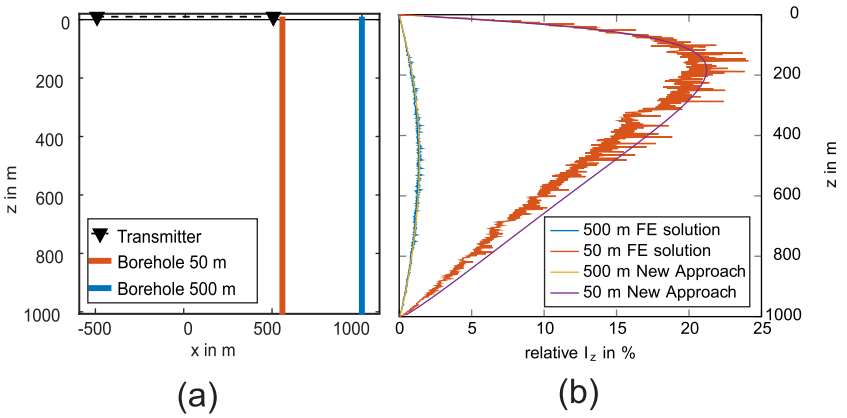

Figure 5. (a) Two wells are placed in 50 and 500 m distance to a 1 km long grounded horizontal electric dipole source. The metal casings were approximated as highly conductive cylinders of 1 m radius, 1 km length, and a conductivity of 5×10^4 S m. Background resistivity is a 3 Ωm half-space. (b) Relative current strength along the two steel casings for a transmitter frequency of 1 Hz. Red and blue lines show results of the finite element simulation, yellow and purple colours indicate results obtained using our new approach.

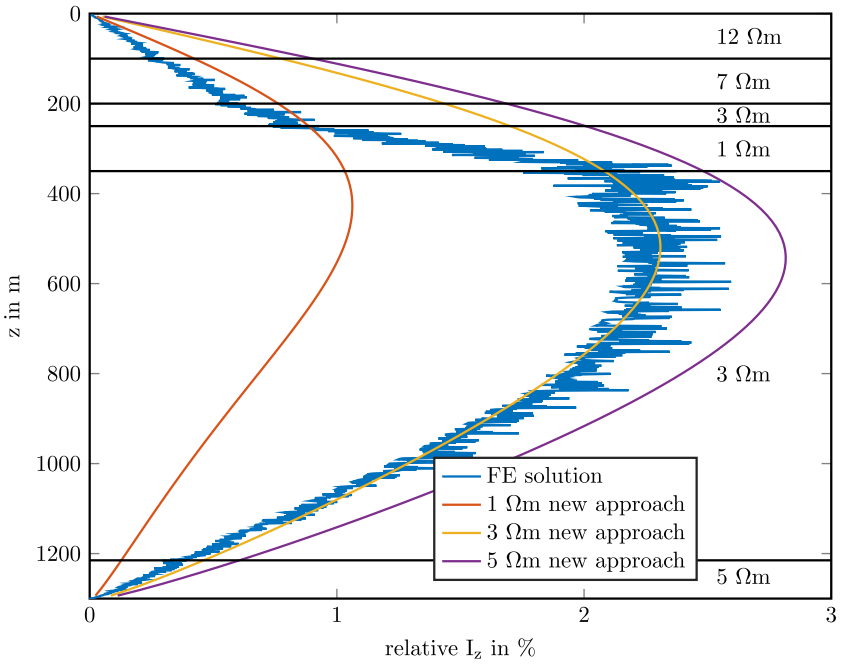

Figure 6. Comparison of current distribution along a conductive cylinder embedded in a layered half-space obtained by finite element simulations (blue colours) and for our algorithm using resistivities of 1, 3 and 5 Ωm. Geometries of the cylinder and transmitter and material properties are as before (see Fig. 4). Layer boundaries are marked by horizontal lines.

on the same axis as the transmitter, again a grounded electric dipole of 1000 m length. The two boreholes were placed in 50 m and 500 m distance from the transmitter. Results are shown in Fig. 5.

As before, the FE simulation shows an influence of numerical noise. Strong currents are observed along the cylinder located close to the transmitter, while currents on the well in 500 m distance are much weaker. For both wells, our algorithm reproduces the shape as well as the amplitude of the current distribution with depth.

Before moving to more realistic 3-D simulations, we would like to point out that our algorithm produces exact solutions only if the boreholes are embedded in a homogeneous half-space. Fig. 6 illustrates the error made when the borehole is embedded in a layered half-space. The blue line in Fig. 6 shows the current distribution along the casing for the same cylinder as in Fig. 4, but now embedded in a 1-D layered half-space with resistivities varying between 1 and 12 Ωm obtained using the finite element approach. The main trend of the current distribution along the casing is similar to the pattern observed for the homogeneous half-space (Fig. 4), with the maximum current strength approximately in the middle of the well at 600 m depth. In contrast to the results for the homogeneous half-space, the current distribution does not follow the same (parabola like) shape as before. For the top 250 m we observe a weaker current, while current strength returns to approximately the same amplitude as in the 3 Ωm example below the conductive layer in 300–400 m depth. The shape of the current distribution along the lower half of the casing does not differ much from results shown before. For comparison, the red, yellow and purple lines show the current distribution obtained with the new approach for half-space conductivities of 1, 3 and 5 Ωm.

A better match of our approach with the FE modelling results for the upper 250 m can be achieved if the half-space is set to 1 Ωm. While a background resistivity of 3 Ωm result in a much better

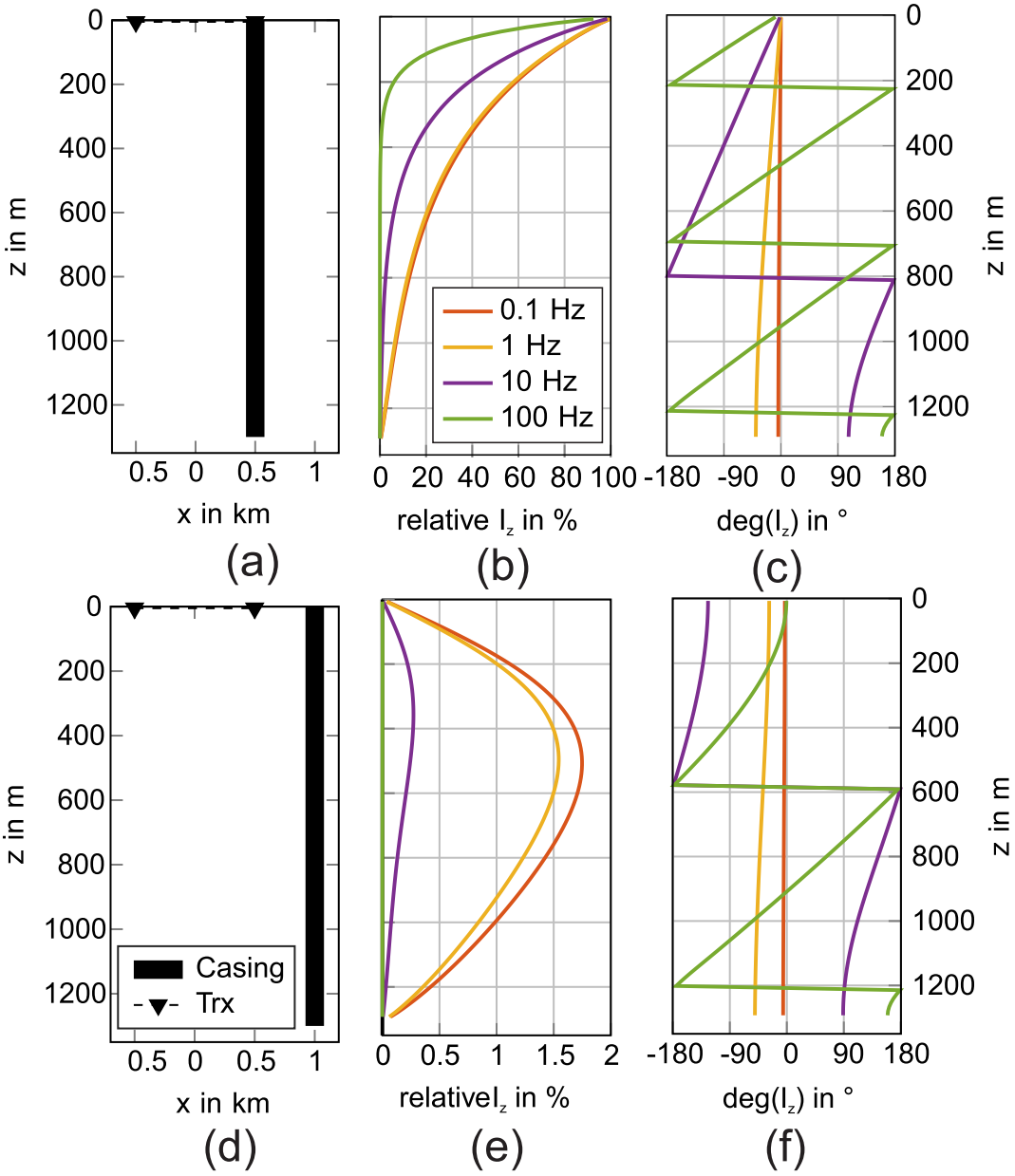

Figure 7. Current distribution on a single steel-cased well embedded in a 3 Ωm half-space for a range of frequencies and two transmitter geometries. In the first scenario (a)–(c), the transmitter is galvanically connected to the transmitter. In the second scenario (d)–(f), the borehole is located at a distance of 500 m from the transmitter. (b) and (e) show the absolute values of the currents along the casing, normalized to the source current strength of the transmitter. (c) and (f) show the corresponding phases of the current along the well.

fit below 400 m. For 5 Ωm the current along the well is overestimated along the entire well. For the layered model shown here, the best overall approximation is obtained for a 3 Ωm half-space, which represents a weighted average of all the layers. Since the 3 Ωm layer is the thickest layer the weighted average is dominated by this value. Testing different scenarios showed that the weighted average results in reasonable approximations of the current. Overall, the approximation with a homogeneous half-space reproduces the first order effect of the steel casing of the layered background. An approximation with a simple half-space model will be generally insufficient if background resistivities are highly variable and particularly for strong contrasts between layers of several orders of magnitude. In other cases and if a good average approximation of the background resistivity structure is chosen the current distribution along the borehole is reproduced.

3.2 Current distribution along steel-cased wells

The current density on steel-cased wells depends not only on material properties of the casing and background resistivity but also on orientation of borehole and transmitter, their distances, frequency of the EM fields and interaction between wells.

In Fig. 7, we show the frequency dependence, using two different borehole transmitter geometries (Figs 7a and d) for galvanically connected (active) and inductively (passive) coupled casings.

For the galvanically coupled casing (Figs 7a–c), the current has full strength of the transmitter at surface and is decreasing exponentially with depth, which is in accordance with results obtained by Yang *et al.* (2009). As can be expected from the skin effect, the decay becomes stronger for increasing frequencies. For low frequencies (0.01 to 1 Hz) saturation is observed, as the DC limit is approached. The phase exhibits a significant shift of up to ±180°

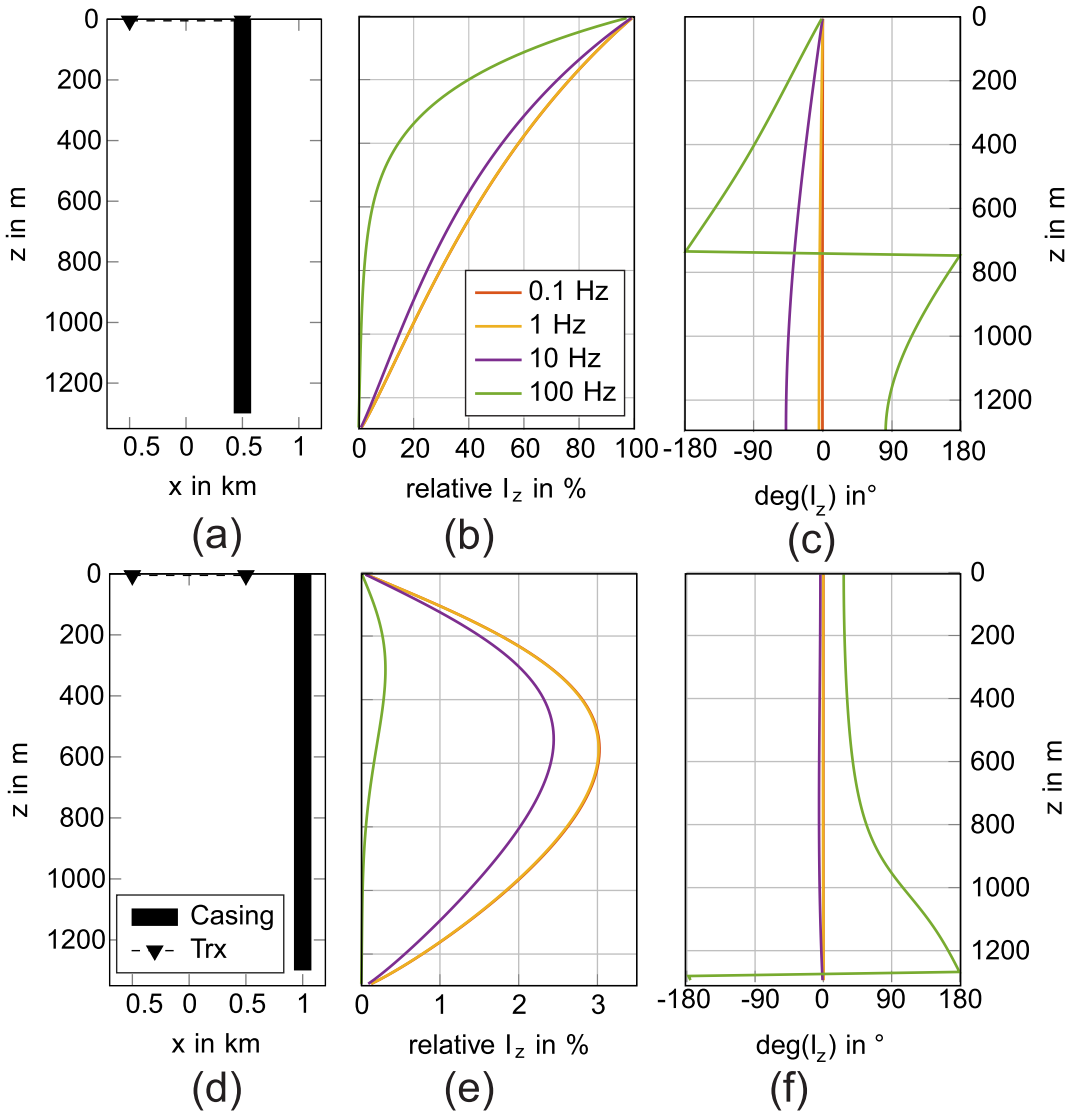

Figure 8. Current distribution on a single steel-cased well embedded in a 30 Ωm half-space for a range of frequencies and two transmitter geometries. In the first scenario (a)–(c), the transmitter is galvanically connected to the transmitter. In the second scenario (d)–(f), the borehole is located at a distance of 500 m from the transmitter. (b) and (e) show the absolute values of the currents along the casing, normalized to the source current strength of the transmitter. (c) and (f) show the corresponding phases of the current along the well.

at higher frequencies, an effect which was not reported by Yang *et al.* (2009). In case of purely inductive coupling (Figs 7d–f), the maximum current strength is reached in about 600 m depths. The depth location of the maximum current strength varies, depending on background resistivity, frequency, transmitter-borehole geometry, and distance. The amplitude generally decreases with increasing frequency but saturation is observed for frequencies of 0.1 Hz and below. As before, phase shifts up to ±180° are observed for high frequencies (10 Hz and above). In general, phase changes along the well result from reversing polarizations of E_z with depth (*cf.* Fig. 3). Increasing the frequency reduces the vertical size of cells of opposite polarity, that is, increasing number of sign reversals of the E_z with depth. A phase shift of the current occurs where E_z changes polarity.

For completeness we calculated the current distribution also for a 30 Ωm half-space using the same setup. Results are shown in Fig. 8.

The general behaviour is very similar to the 3 Ωm half-space. However, for the galvanically coupled well (Figs 8b and c) the decay is much slower than for a more conductive background (*cf.* Figs 7 b and e). This finding is in agreement with results reported earlier by Yang *et al.* (2009). Saturation of current amplitudes and phase shifts appear at lower frequencies than before. Similar observations are made for the inductively coupled wells shown in Figs 8(e) and (f). The absolute value of the current is twice as strong as for the 3 Ωm half-space, the saturation point in the current strength and the phase shifts appear at lower frequencies.

Next, we investigate the influence of the orientation of steel-cased wells to the transmitter. Therefore, we placed a borehole at angles between 0 and 180 degree to the transmitter axis (Fig. 9a).

As described previously for inductively coupled wells, the amplitude of the current vanishes at the top and the bottom of the well (Fig. 9b). The amplitude of the maximum current however, depends significantly on the borehole-transmitter orientation. Strongest currents are obtained when the transmitter is placed in line with the borehole (0°). A deviation of only 30° reduces the current strength by a factor of two. If the borehole is placed perfectly perpendicular to the transmitter-axis the current along the casing vanishes completely since there is no vertical electric field produced by the trans-

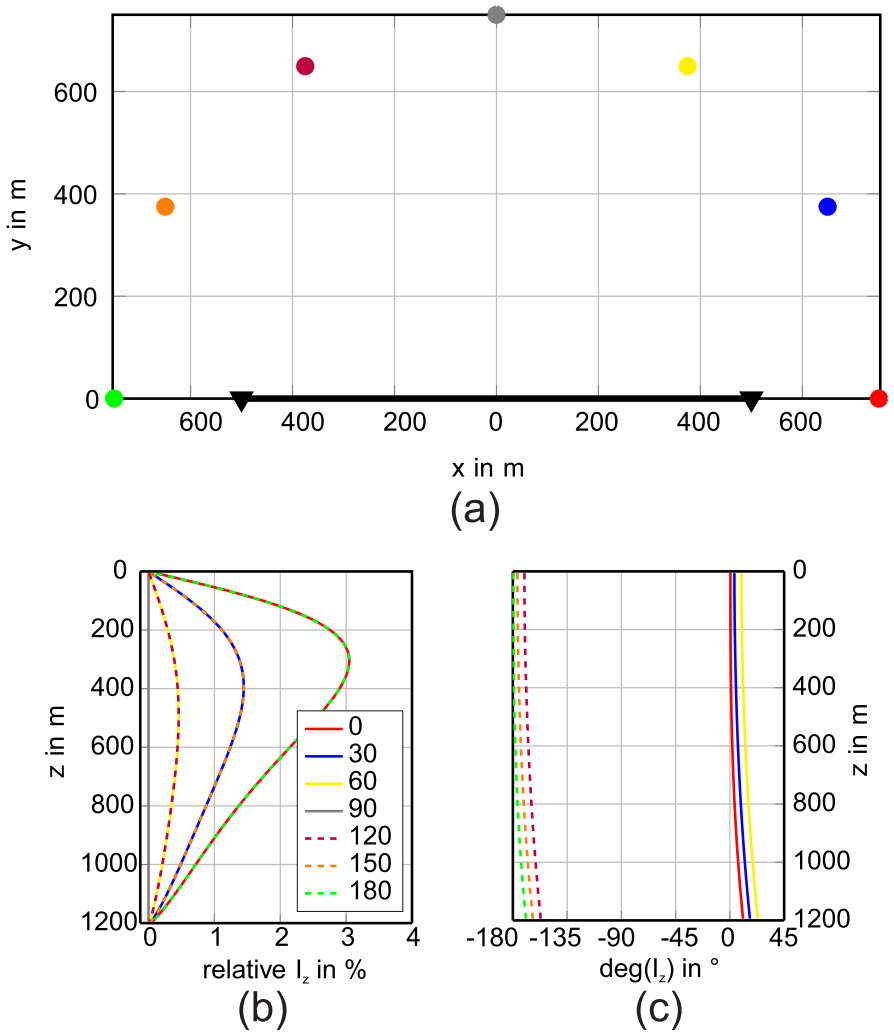

Figure 9. Influence of varying orientation between borehole and transmitter axis on current distribution. The background model is a 3 Ωm half-space, the frequency used is 1 Hz. (a) A 1 km long grounded electric dipole is used as transmitter (black). The distance between steel-cased well to the centre point of the transmitter is 750 m, the angle varies from 0° to 180°. All steel-cased wells are 1200 m long and have a diameter of 18 cm. The casings are 1 cm thick, have a conductivity of 5×10^6 S m^{-1}, and were divided into 100 segments. (b) Absolute value of the current strength along the steel casing for varying angles to the transmitter normalized to the current strength of the transmitter. (c) Phase of the obtained current along the borehole casing.

mitter that could give rise to currents along the casing (see Fig. 3d). The 180° switch in phase is caused by the change in polarity of the background field as shown in Figs 3(c) and (d).

Fig. 10 compares results for a borehole aligned with the transmitter axis and varying borehole-transmitter distances. The wells are located between 10 and 610 m away from the end of the transmitter. All other parameters are the same as before. Fig. 10(a) shows that the amount of current induced into the casing reduces quickly with increasing distance of the well from the transmitter. If the current is injected only 10 m away from the casing, currents on the casing reach up to 40 per cent of the injected transmitter currents within the upper 300 m of the casing. At distances greater 310 m, induced currents do not exceed 1 per cent. Larger phase shift occur with increasing distance (Fig. 10d), which can be explained by an increase in the phase shift of the primary field for larger distances (*cf.* Figs 3c and d).

If we now assume that not only one of the boreholes in Fig. 10 is present but all six of them, interaction between all wells must be considered. Results are shown in Figs 10(b) and (e). As a result of interaction between the wells, induced current along each of the boreholes becomes smaller than for single wells. However, the reduction is not evenly distributed between the boreholes. Current strength is only little reduced for the casing closest to the transmitter. For all other wells the intensity of the current is reduced by a factor of two. This can be explained by a mixture of different effects. As the total amount of energy in the system is maintained, the currents are distributed between all wells. Since most of the energy is consumed in wells closest to the transmitter, less energy is available for wells with larger distance to the transmitter, and hence the amount of current decreases accordingly. The effect is strongest if the first well is galvanically connected to the transmitter as shown in Fig. 10(c).

3.3 3-D Example

In order to investigate the effect of steel-cased wells in a 3-D simulation, we show a synthetic example of a simplified oil reservoir. The geometry of the modelling domain is shown in Fig. 11. The 3-D reservoir is located at 1200 m depth and measures $1000 \times 1000 \times 15$ m^3. The resistivity of the reservoir is 16 Ωm, which represents a situation where the oil has been partly replaced

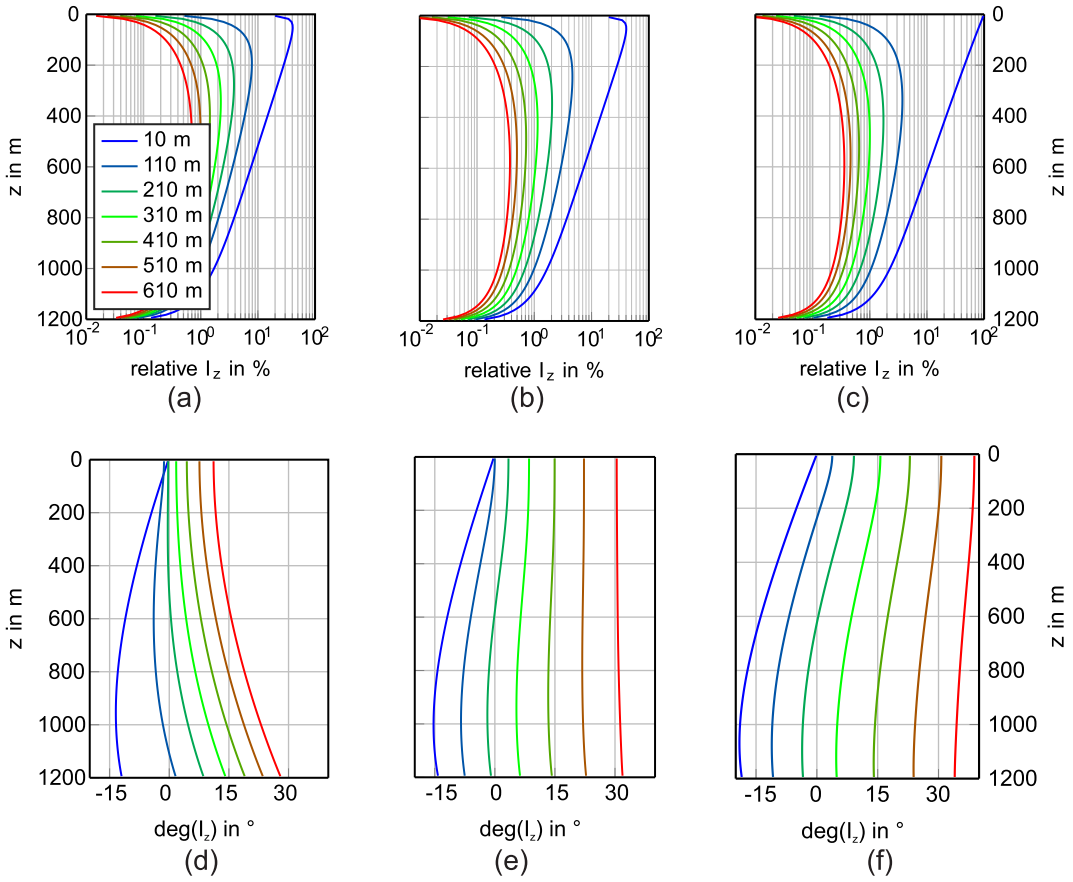

Figure 10. Current distribution with depth along steel-cased wells for varying transmitter-borehole distances. The transmitter is a grounded electric dipole of 1 km length. Simulations are calculated for a frequency of 1 Hz and a background resistivity of 3 Ωm. The steel casing is placed in line with the transmitter axis. For (a) and (d), currents were calculated neglecting interaction between wells. In all other calculations interaction between wells is considered. In (b) and (e), current was injected at 10 m distance to the closest well, while in (c) and (f) the steel casing of the first well was galvanically connected to the transmitter. Note the logarithmic scale of the I_z axis in (a)–(c).

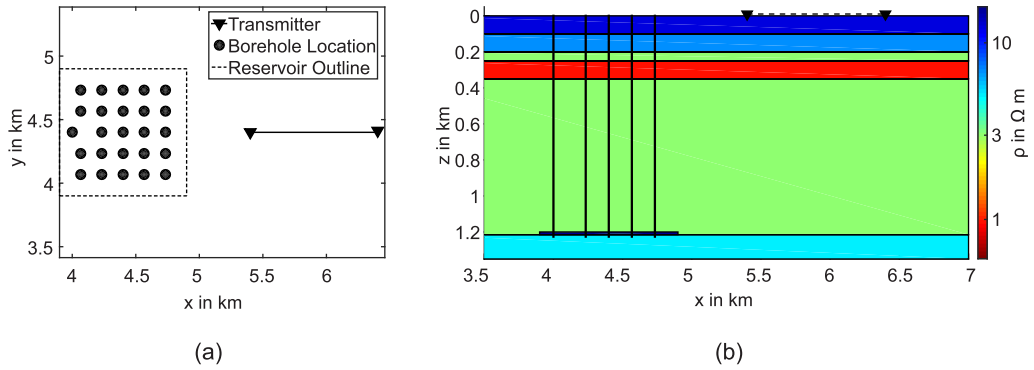

Figure 11. 3-D reservoir model including 25 steel-cased wells. (a) Map view of the transmitter borehole geometry in relation to the reservoir. (b) Vertical slice through the conductivity model along the axis of the transmitter at $y = 4.4$ km.

by formation water. The background of the model is a layered half-space as used before (Fig. 6). A 1 km long grounded electric dipole is placed at surface as transmitter. The reservoir is penetrated by 25 steel-cased wells with horizontal distances of 166 m.

Horizontal electric fields were calculated for two scenarios: At first the effect of the steel-cased wells were neglected; for the second scenario all 25 wells including their interaction were taken into account. Computations are performed for a frequency of 0.1 Hz. Fig. 12 shows the relative changes of the electric field in the x-direction at surface due to the 25 wells.

The boreholes closest to the transmitter produce an increase in the electric field amplitudes (red colours), while all other boreholes seem to decrease the E_x amplitudes. Since the shortest borehole-transmitter distance is more than 500 m (*cf.* Fig. 10) the current on each of the wells is rather small (<3 per cent of the transmitter current). Moreover, the electric field in the x-direction at the location of the wells is much larger than E_z. Nevertheless the influences of the steel-cased wells are significant, not only in the close vicinity to the boreholes but also at greater distances of up to several kilometres. In the area directly above the reservoir, electric field values decrease

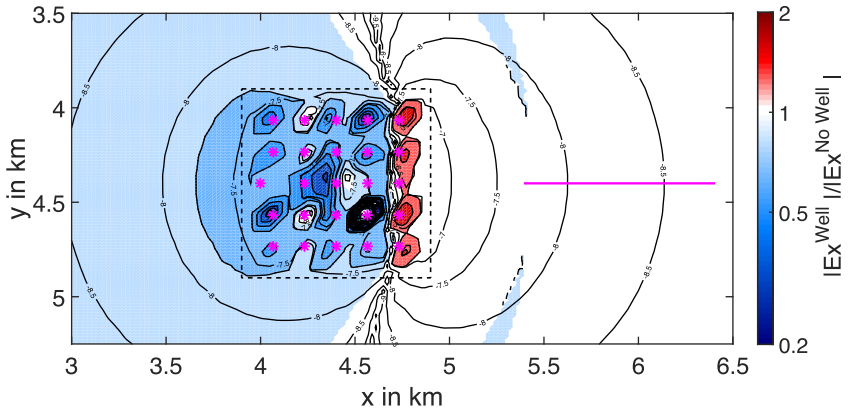

Figure 12. Distortion of the electric field in the *x*-direction at surface, caused by the presence of 25 steel-cased wells. The location of the boreholes is marked by purple asterisks. All boreholes reach 1300 m depth and penetrate the reservoir. The background resistivity used to calculate the current strength along the boreholes is 3 Ωm. The location of the transmitter is indicated by a purple line. Colours represent the ratio of the electric field obtained for simulations including boreholes and simulations without steel casings. Black isolines show absolute values of the electric field on a log-scale, which is produced by the boreholes. Computations are for a frequency of 0.1 Hz.

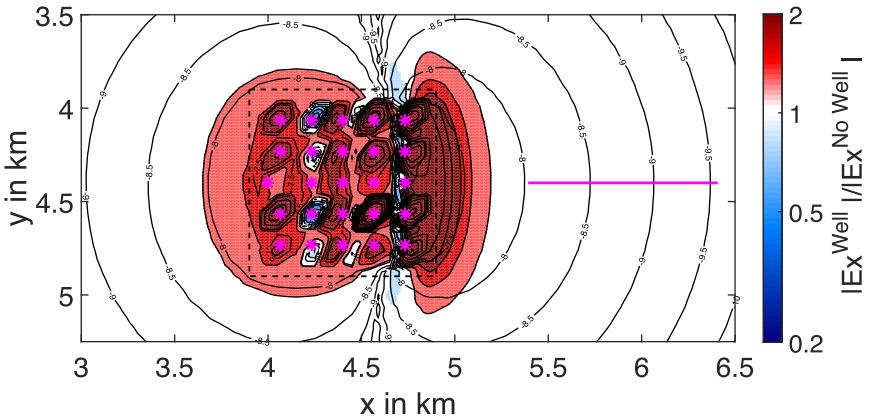

Figure 13. Distortion of the electric field in the *x*-direction at reservoir level, caused by the presence of 25 steel-cased wells. The location of the boreholes is marked by purple asterisks. All boreholes reach 1300 m depth and penetrate the reservoir. The background resistivity used to calculate the current strength along the boreholes is 3 Ωm. The location of the transmitter is indicated by a purple line. Colours represent the ratio of the electric field obtained for simulations including boreholes and simulations without steel casings. Black isolines show absolute values of the electric field on a log-scale, which is produced by the boreholes. Computations are for a frequency of 0.1 Hz.

by up to 40 per cent and even at a distance of 1 km from the wells, the field values drop by 10 per cent. This result clearly shows that steel-cased wells must be considered for 3-D CSEM modelling.

Finally we consider the electric field in the *x*-direction for the same simulation, but now at reservoir depth (Fig. 13). At reservoir level, steel-cased wells increase the amplitude of the electric fields significantly. The relative impact of the boreholes is much larger than at surface because E_x generated by the surface transmitter decays with depth and thus the secondary E_x field generated by the boreholes is relatively larger. Near the centre of the reservoir, the electric fields increase by 100 per cent but the effect is even stronger towards the right edge of the reservoir. This seems plausible because the strongest currents are found on boreholes closest to the transmitter, which is located to the right of the reservoir (see Fig. 11). In comparison to the effect observed at surface, the influence of the steel casings seems to be concentrated more to the region of the boreholes.

4 INFLUENCE ON SENSITIVITY

Since steel casings do significantly influence the electric field distribution over large volumes, it can be expected that sensitivity of any CSEM inversion is affected as well. We implemented the borehole solution described in the previous section into our 3-D CSEM inversion code described by Grayver *et al.* (2013). We used this algorithm to calculate the sensitivity for the model setup shown in Fig. 14. We used the same general conductivity structure of the reservoir in a layered half-space. In contrast to the 3-D simulation discussed before, we only use a single metal casing. In addition the transmitter is moved from the right side of the reservoir to the left. The steel-cased well is not galvanically connected to the transmitter but placed 20 m away from the grounding point of the transmitter. We used 25 receivers placed on a regular grid (distance 900 m) above the reservoir.

Starting from the explicitly calculated Jacobian J we computed the cumulative sensitivity as follows:

$$J_{cj} = \frac{1}{V_j} \sum_{i=1}^{N_d} |J_{i,j}|^2 \; i = 1, \ldots, N_d, \, j = 1, \ldots, N_m. \tag{14}$$

N_d is the number of data points, N_m the number of model cells considered during inversion, and V_j the volume of each grid cell. Dividing the elements of J by the corresponding cell volumes V_j cancels out the effect of the irregular grid sizes. The resulting cumulative

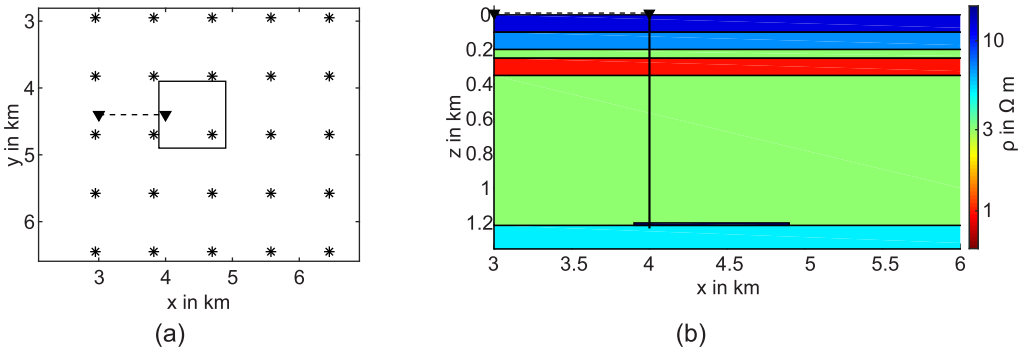

Figure 14. Model setup used to calculate the effect of a single steel casing on the sensitivity distribution of 3-D inversion. (a) Map view of the source receiver geometry in relation to the reservoir. In total 25 receivers are used. The transmitter is a 1 km long horizontal dipole. (b) Vertical slice through the conductivity model along the axis of the transmitter. The background model is a layered half-space. A 16 Ωm reservoir of 1000 × 1000 × 15 m^3 was placed at a depth of 1200 m. The steel casing reaches from surface to a depth of 1226 m, penetrating the reservoir. The casing has a diameter of 16 cm and a thickness of 1 cm. The casing is placed 20 m away from the right grounding point of the transmitter.

sensitivity J_{cj} shows the influence of one model cell summed with respect to all data components.

Similarly to the results shown for the 3-D forward simulation example, we calculated cumulative sensitivities for the two scenarios with and without steel-cased well. The normalized absolute value of the sensitivity neglecting the presence of steel-cased wells, is shown in Fig. 15(a). The change in sensitivity due to the presence of a borehole at a distance of 20 m from the transmitter is shown in Fig. 15(b). For completeness Fig. 15(c) shows results if the transmitter is galvanically connected.

In general, highest sensitivity is found close to surface with maximum values at the location of the current electrodes of the transmitter but sensitivity decreases drastically with depth (Fig. 15a). At reservoir level the sensitivity is about 5 orders of magnitude smaller than at surface. Unexpectedly low sensitivities are found for the conductive layer between 250 and 350 m depth. Overall, in presence of a single steel-cased well, sensitivity increases in the model domain at greater depth but is reduced at surface (blue colours at surface). This general pattern holds for a *passive* well at a distance of 20 m from the transmitter (Fig. 15b) and a galvanically connected well (Fig. 15c). Higher amplitudes of sensitivity are observed for the latter scenario. Figs 15(b) and (c) also show that sensitivities do not only change in vertical direction, but also laterally. Immediately behind the casing, sensitivity decreases as currents are deflected inside the casing. At further distance from the well, a reduction in sensitivity is mainly observed above and below the conductive layer (indicated by black lines) but not inside the conductive layer. At surface sensitivity is reduced by 50 per cent for the inductively coupled well and by up to 90 per cent in the vicinity of the point where the transmitter is connected to the casing. At reservoir level, on the other hand, sensitivity increases by 100 per cent and more for both scenarios over large volumes (see Fig. 15c). This increase of sensitivity with depth can be exploited for exploration or monitoring purposes. The increase of sensitivity at depth is not limited to the vicinity of the well but extends to depths beyond 1 km below the reservoir. While the steel casing leads to an increase in sensitivity at depth, the absolute values of sensitivity are still fairly low.

5 DISCUSSION

Our algorithm is based on a number of minor and major limitations and assumptions.

First, the calculation of the source currents is limited to a homogeneous half-space as background. The true distribution of current with depth changes, however, if the background model is more complex. Comparing results for homogeneous and layered half-spaces using FE simulations (see Fig. 6), we found that our approach can still describe first order effects of steel casings if the background conductivity model is chosen appropriately, that is, as an average of the layered background resistivity. This restriction could be addressed by using the Green's tensor element of a layered half-space in eq. (3). However most (semi-) analytic formulations for VED sources in layered half-spaces (e.g. Streich & Becken 2011) make use of reflection coefficients between layer boundaries, which are dependent on the source depth, making the analytic integration over vertically extended sources difficult.

Steel-cased wells are described by a number of dipole source elements. Some of these dipole elements are located within a cell whose conductivity differs from the conductivity used to calculate the primary field. Therefore singularities at the source position are not completely removed from the secondary field. One should be aware that in certain circumstances this can cause accuracy problems.

Our solution works only for perfectly vertical boreholes. This limits applicability of the approach as many boreholes are typically drilled from one platform into various directions along complex trajectories. If the transmitter is far away from the well, and the well trajectory is mostly vertical in its upper part, the influence of the bended lower part can be expected to be relatively small, since background field amplitudes decrease rapidly with distance to the transmitter. To properly address deviated well-trajectories, it would be necessary to integrate the entire Green's tensor over tilted cylinder volumes instead of only the *zz*-component. This would also allow inclusion of other steel infrastructure, such as pipelines, into CSEM modelling. However, analytic integration of all nine components of the Green's tensor over tilted cylinder volumes will be complicated and the use of numerical integration techniques may be more suitable. Using numerical integration techniques, though, would require the calculation of a tremendous amount of Hankel transformations which is likely to be numerically time consuming.

We also assumed the casing to be non-magnetic, which is generally not true. Particularly at higher frequencies, horizontally aligned eddy currents inside the casing will occur. One could think of describing this effect by substituting the casing by a series of vertical magnetic dipoles. Horizontally aligned eddy currents inside the casing can then be seen as source currents of horizontally aligned loops corresponding to vertical magnetic dipole sources. However,

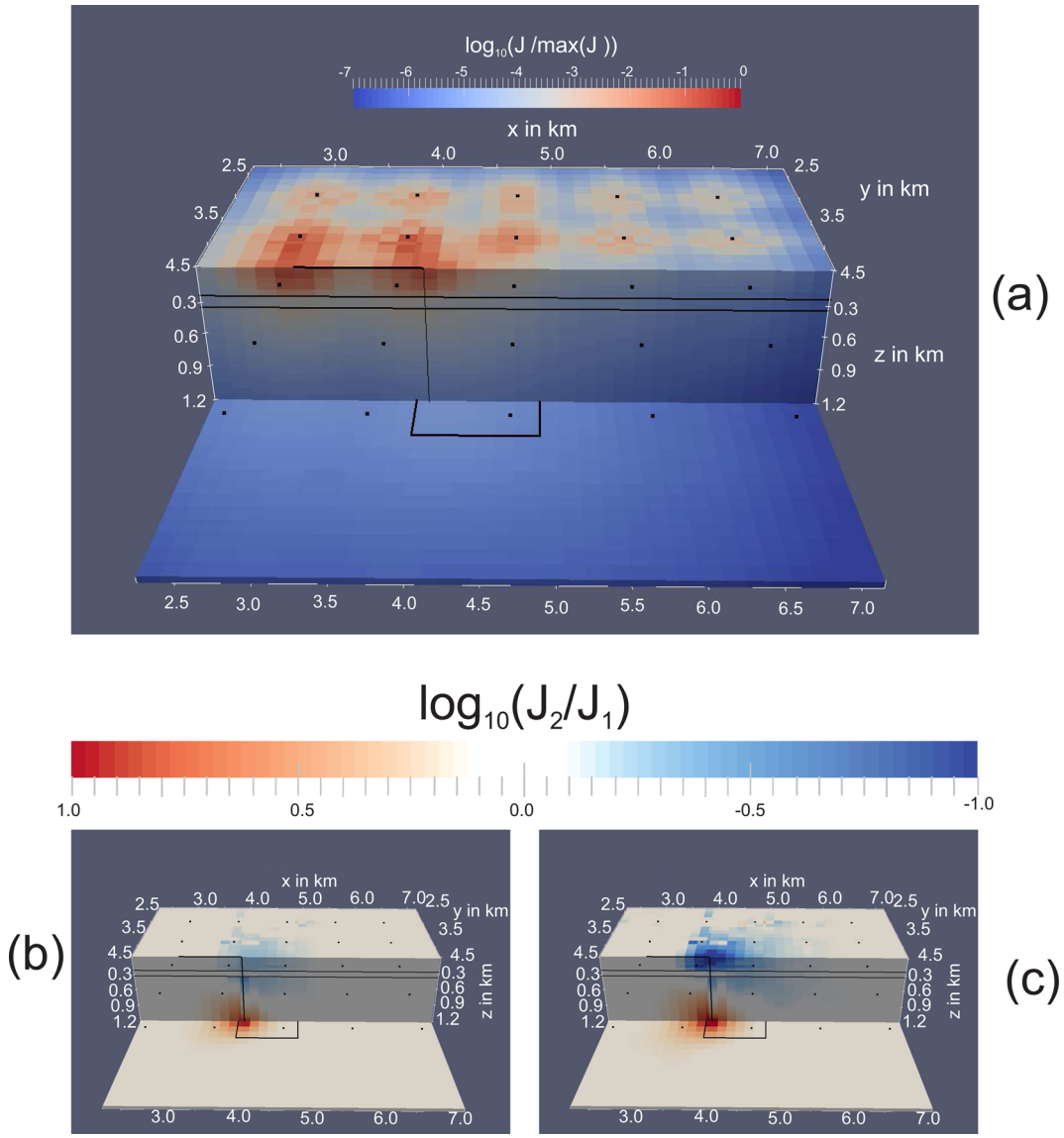

Figure 15. (a) Normalized absolute cumulative sensitivity for the model setup shown in Fig. 14, neglecting the presence of the steel-cased well. (b,c) Relative change of the cumulative sensitivity due to the presence of the steel-cased well for the model setup shown in Fig. 14. Results are obtained for a single frequency of 0.1 Hz. Background field used to calculate the current strength is 3 Ωm and the casing was divided into 100 segments of equal length. (b) Considering a passive borehole at a distance of 20 m from the transmitter. (c) Considering a galvanic connection between transmitter and casing.

this would require the knowledge of the magnetic permeability of the steel used which is often poorly constrained. For low frequencies (<100 Hz), which are typically used for CSEM exploration or monitoring applications, however, associated eddy currents are probably small and can be neglected. Another unknown is the contact resistance between steel, cement and surrounding rock, which can also change over time if steel and/or cement corrode.

6 CONCLUSIONS

The presented method describes the first order effects of steel-cased wells including interaction between multiple wells, which is essential for hydrocarbon exploration and monitoring applications with hundreds of wells in an oil field. Metal casings can be described as part of the primary field by replacing them with a series of substitute dipoles, whose dipole moments are calculated from the primary field of the transmitter. As no assumptions on type and orientation of the transmitter are made, the new algorithm can be easily adopted to any EM scenario and EM simulation where a secondary field approach is used.

The presence of steel-cased wells has a significant effect on the distribution of the electromagnetic fields in the subsurface. The effect is highly dependent on borehole-transmitter orientation, distance and frequency. Influence of steel casings is not limited to the close vicinity of the boreholes but can be seen even at distances of up to 2 km. Our results do not only have implications for the modelling and inversion of CSEM data but they should be considered at the planning stage of CSEM surveys. In areas where steel-cased wells are present, casings can be used as galvanically coupled source extensions that carry the current to greater depth. The current along the well decays exponentially until it reaches zero at the bottom of the well. If multiple wells are present it may therefore be advantageous to use the one having the greatest penetration

depth. In order to obtain stronger currents at the depth of investigation. Sensitivity can increase by more than 100 per cent near the bottom of the steel-cased wells (which are usually located close to the reservoir). If galvanic coupling is not possible due to logistics or safety issues, it may still be useful to set up a transmitter inline and as close as possible a steel-cased borehole. Since the amount of current induced along the casing is still significant as long as the distance between casing and transmitter is small these currents will increase the overall sensitivity to the reservoir structures.

ACKNOWLEDGEMENTS

This research work was funded by Wintershall Holding GmbH, Kassel (Germany). We particularly acknowledge continuous support from Bert Verboom and Paul Veeken. We would like to thank further the reviewer Michael Commer for his comments which significantly improved the manuscript.

REFERENCES

Augustin, A.M., Kennedy, W.D., Morrison, H.F. & Lee, K.H., 1989. A theoretical study of surface-to-borehole electromagnetic logging in cased holes, *Geophysics,* **54**(1), 90–99.

Commer, M., Hoversten, G.M. & Um, E.S., 2015. Transient-electromagnetic finite-difference time-domain earth modeling over steel infrastructure, *Geophysics,* **80,** 147–162.

Constable, S., 2010. Ten years of marine CSEM for hydrocarbon exploration, *Geophysics,* **75**(5), A67–A81.

Frischknecht, F.C., 1988. *Electromagnetic Physical Scale Modeling,* Society of Exploration Geophysicists, chap. 6, pp. 364–441.

Grayver, A.V., Streich, R. & Ritter, O., 2013. Three-dimensional parallel distributed inversion of CSEM data using a direct forward solver, *Geophys. J. Int.,* **193**(3), 1432–1446.

Newman, G.A. & Alumbaugh, D.L., 1997. Three-dimensional massively parallel electromagnetic inversion – I. Theory, *Geophys. J. Int.,* **128,** 345–354.

Orange, A., Key, K. & Constable, S., 2009. The feasibility of reservoir monitoring using time-lapse marine CSEM, *Geophysics,* **74**(2), 21–29.

Pardo, D., Torres-Verdín, C. & Zhang, Z., 2008. Sensitivity study of borehole-to-surface and crosswell electromagnetic measurements acquired with energized steel casing to water displacement in hydrocarbon-bearing layers, *Geophysics,* **73,** F261–F268.

Raiche, A.P. & Coggon, J.H., 1975. Analytic Green's Tensors for Integral Equation Modelling, *Geophys. J. R. astr. Soc.,* **42,** 1035–1038.

Rocroi, J.P. & Koulikov, A.V., 1985. The use of vertical line sources in electrical prospecting for hydrocarbon, *Geophys. Prospect.,* **33**(1), 138–152.

Siemon, B., Christiansen, A.V. & Auken, E., 2009. A review of helicopter-borne electromagnetic methods for groundwater exploration, *Near Surf. Geophys.,* **7,** 629–646.

Streich, R., 2009. 3D finite-difference frequency-domain modeling of controlled-source electromagnetic data: direct solution and optimization for high accuracy, *Geophysics,* **74,** 95–105.

Streich, R. & Becken, M., 2011. Sensitivity of controlled-source electromagnetic fields in planarly layered media, *Geophys. J. Int.,* **187,** 705–728.

Swidinsky, A., Edwards, R.N. & Jegen, M., 2013. The marine controlled source electromagnetic response of a steel borehole casing: applications for the NEPTUNE Canada gas hydrate observatory, *Geophys. Prospect.,* **61,** 842–856.

Tang, W., Li, Y., Swidinsky, A. & Liu, J., 2015. Three-dimensional controlled-source electromagnetic modelling with a well casing as grounded source: a hybrid method of moments and finite element scheme, *Geophys. Prospect.,* **63,** 1491–1507.

Tietze, K., Ritter, O. & Veeken, P., 2015. Controlled-source electromagnetic monitoring of reservoir oil saturation using a novel borehole-to-surface configuration, *Geophys. Prospect.,* **63,** 1468–1490.

Wait, J.R. & Hill, D.A., 1973. Excitation of a homogeneous conductive cylinder of finite length by a prescribed axial current distribution, *Radio Sci.,* **8**(12), 1169–1176.

Wirianto, M., Mulder, W.A. & Slob, E.C., 2010. A feasibility study of land CSEM reservoir monitoring in a complex 3D-model, *Geophys. J. Int.,* **181,** 741–755.

Yang, W., Torres-Verdín, C., Hou, J. & Zhang, Z., 2009. 1D subsurface electromagnetic fields excited by energized steel casing, *Geophysics,* **74,** E159–E180.